Short Papers

Lateral Vehicle State and Environment Estimation Using Temporally Previewed Mapped Lane Features

Alexander A. Brown and Sean N. Brennan

***Abstract*—This paper proposes a model-based method to estimate lateral planar vehicle states using a forward-looking monocular camera, a yaw rate gyroscope, and an *a priori* map of road superelevation and temporally previewed lane geometry. Theoretical estimator performance from a steady-state Kalman-filter implementation of the estimation framework is calculated for various look-ahead distances and vehicle speeds. The application of this filter structure to real driving data is also explored, along with error characteristics of the filter on straight and curved roads, with both superelevated and flat profiles. The effect of superelevation on estimator performance is found to be significant. Experimental and theoretical analysis both show that the benefits of state estimation using previewed lane geometry improve with increasing lane preview, but this improvement diminishes due to increased lane tracking errors at distances beyond 20 m ahead of the vehicle.**

***Index Terms*—Bayes methods, dead reckoning, Global Positioning System, inertial navigation, road vehicles, robot vision systems, sensor fusion, simultaneous localization and mapping, state estimation, vehicle dynamics.**

I. Introduction

Knowledge of a vehicle's previewed reference trajectory is central to effective lateral and longitudinal vehicle guidance, and ever since the first successful attempts at autonomous driving many researchers and practitioners alike have made use of forward-facing cameras for vehicle environment and ego-perception [1]–[13]. The fundamental challenge of using vision-based systems for vehicle guidance is that normal driving scenes can experience clutter, changing lighting conditions, and severe occlusions; the premise of this work is that a map-referenced temporal feature horizon with a relative motion model for the road can significantly improve the robustness of vision-based vehicle state estimation.

A review of vision-based vehicle guidance systems [13] reveals a mixture of approaches. Some of these methods are computationally simple and generally effective but do not make use of mapped information to aid camera systems in their perception of the environment or vehicle states [1]–[4], [14], [15]. Recently, researchers have sought to combine cameras with map information to improve vehicle localization, tracking, state estimation, and environment perception [6]–[12], [16]. Others have used simultaneous localization and mapping (SLAM) [17], [18] iterative searching [7], and similar algorithms. For example, the work in [18] relies on corner-type features for environment and ego-perception. The work in [17] uses instead an ingenious method for motion recovery based on a biologically inspired optical-flow-based method. While these camera-based methods (similar to laser-based methods [19], [20]) hold great promise in research settings, they pose problems in practical implementation due to the computational complexity of the filtering and measurement processes. Furthermore, it can be challenging to predict the algorithm performance in practice as this depends strongly on how many mapped features are available for recognition by the forward-looking sensors at any given moment.

This paper complements the results presented in [21], which considered map-aided localization in the longitudinal direction using very low-dimensional maps and pitch measurements. In particular, this paper addresses the possibility of treating the longitudinal and lateral estimation problems as independent by developing a lightweight map-based lateral state estimator meant to operate using longitudinal registration provided by a separate process. The lateral state and environment model used in this paper is inspired by the work of Sharp and Valtetsiotis in [22], which offers a unique look at preview-based lateral vehicle control. The key contribution of this paper is that it combines elements of the aforementioned ideas into a generic time-varying Kalman-filter framework for a predictive vehicle state estimator. This method is unique in that it leverages mapped road geometry without tightly coupling longitudinal and lateral position estimation by using the temporal preview concept, allowing for a much simpler Kalman-filter estimator structure, similar to estimators already regularly used within chassis-control engine control unit (ECU) systems. For the sake of redundancy and reliability, it specifically combines information from three sources: vehicle dynamic models, measurements from a forward-looking camera and yaw rate gyroscope for measurements, and a map of the right lane edge's position. This estimator is then used to establish a concrete relationship between camera look-ahead distance and theoretical estimator performance. The vehicle model used is linear, the measurements of previewed road points are accomplished using a monocular camera, and suspension motion is neglected as a source of error, but the quality of the experimental results supports these simplifications. In the form presented here, this estimator is likely limited in application to situations where contributions of longitudinal dynamics, suspension movement, and other nonlinearities to overall vehicle motion are small, such as normal highway driving under cruise control.

The remainder of this paper is organized as follows. First, the estimation framework is derived in two parts: the vehicle model is introduced and then the temporal road motion model is derived. Following this, equations are presented that combine road and vehicle motion equations into an augmented discrete state-space system. Next, the overall estimator architecture based on this combined system is described. The integration of the Kalman filter with the map in the form of a state input is given, followed by the description of the camera measurement noise model. A discussion follows of the theoretical estimator performance for varying speeds and preview distances. The paper concludes with an experimental implementation of the filter framework and analysis of these results.

Manuscript received June 25, 2013; revised January 6, 2014, May 27, 2014, and September 16, 2014; accepted October 24, 2014. The Associate Editor for this paper was S. Birchfield.

The authors are with the Department of Mechanical and Nuclear Engineering and the Larson Transportation Institute, Pennsylvania State University, University Park, PA 16802 USA (e-mail: alexanderallenbrown@gmail.com).

Color versions of one or more of the figures in this paper are available online at http://ieeexplore.ieee.org.

Digital Object Identifier 10.1109/TITS.2014.2366991

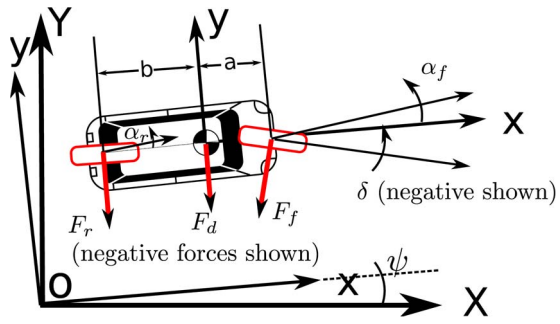

Fig. 1. Setup of planar vehicle dynamic equations.

II. Estimator Formulation

The dynamic equation used to describe the motion of the combined road–vehicle system used in this paper is similar in structure to the one proposed in [22] as a basis for an optimal preview controller for lateral vehicle state control and path following. The reader is referred to [22]–[24] for a more detailed discussion of this preview-based control structure. The basic idea of this approach is to use a temporal horizon containing control-relevant information in the form of a previewed reference trajectory. This allows an linear quadratic regulator (LQR)-type controller to achieve anticipatory behavior and has proven successful in replicating human driver behavior even at high speeds. In this paper, the same concept is employed to improve vehicle state estimates for control purposes using low-cost sensors. In [25], the authors introduced two versions of the preview estimator framework: the first, derived in global coordinates, is a direct analog to Sharp and Valtetsiotis' work in [22]. While the global coordinate formulation has stronger ties to the literature, this paper focuses on the more easily implemented body-fixed version of the estimator, derived hereinafter.

A. Vehicle Model

To maintain this work's focus on a simple but effective lateral vehicle state estimation scheme, the familiar "bicycle model" for vehicle dynamics is employed. The relevant coordinate systems, angles, and tire forces are shown in Fig. 1.

The vehicle-referenced linear bicycle model equations in the International Standards Organization (ISO) body-fixed coordinates with x forward, y left, and z up are given below in (1).[1] See [26] for a complete derivation. This model neglects suspension motion and lumps tire forces from front and rear tires into one effective tire at each axle, but it has been proven accurate enough for lateral vehicle control under nominal conditions in experimental testing. In the literature, it has also been used with modifications to the linear tire model to describe extreme high sideslip maneuvers, as in [27]. Because this study is focused on highway or rural road constant-speed driving, tire forces are assumed linear with constant cornering stiffness for each. This is certainly a significant simplification, but the results section will show its validity for the nonemergency driving scenarios considered and with the cornering stiffnesses obtained from system identification experiments. The equations are presented in state-space form in (1) as functions of effective cornering stiffnesses C_f, C_r, mass and yaw moment of inertia m and I_z, forward speed U, lateral velocity V, yaw rate $r = (d\psi)/(dt)$, road superelevation e, and b, a, δ defined as in Fig. 1 by

$$\begin{bmatrix} \dot{V} \\ \dot{r} \end{bmatrix} = \begin{bmatrix} \frac{-(C_f+C_r)}{mU} & \frac{bC_r-aC_f}{mU} - U \\ \frac{bC_r-aC_f}{I_zU} & \frac{-(a^2C_f+b^2C_r)}{I_z} \end{bmatrix} \begin{bmatrix} V \\ r \end{bmatrix} + \begin{bmatrix} \frac{C_f}{m} & -g \\ \frac{aC_f}{I_zU} & 0 \end{bmatrix} \begin{bmatrix} \delta_f \\ e \end{bmatrix}. \quad (1)$$

[1]The coordinate system defined is in ISO 8855:2011.

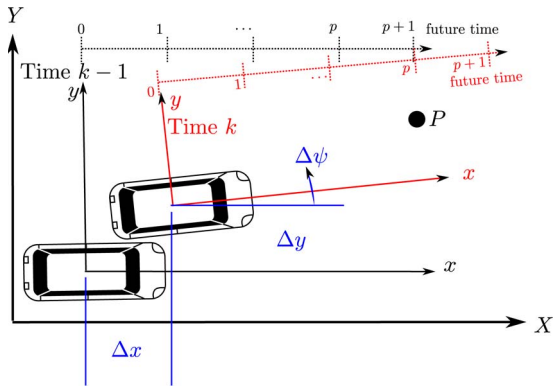

Fig. 2. Relative road movement from time step $k-1$ to k.

This state-space representation of the vehicle dynamic equations is discretized using a Tustin transform approximation so that the states become sampled representations of lateral velocity and yaw rate, V_k and r_k. These equations for local lateral velocity and yaw rate are independent of the road geometry in the xy plane, and the only influence that the road has on the states is through the superelevation e. The equation also assumes that the direction of V changes as the vehicle rotates, which is convenient for a motion model with measurements provided by a sensor attached to the vehicle.

B. Road Edge Motion Model

Similar to the model for road motion presented for use in an optimal preview controller in [22], the world around the vehicle is modeled as a set of points that moves past the vehicle with a known velocity. Each of these is a state in the state vector of the combined vehicle-road motion equations, presented later in (7). Instead of tracking individual features according to their spatial relationship to the vehicle, each point on the road ahead is assigned a *future time step*. The representation of spatially distant road features as features that will pass under the vehicle at a known future time is technically noncausal. Measurements from the future are not available, but when vehicle speed is known and constant and when the vehicle remains in its lane, the road's future position in time can be predicted with reasonable accuracy. This, in turn, allows the state-space equations for the vehicle-road system to remain linear and eliminates the need for the filter to track both x and y locations for each previewed road point. This is a fundamental simplification of SLAM. The derivation for this relationship is given hereinafter.

The key to the temporal horizon concept is that road points in the state vector are assumed to move relative to the vehicle based on its local velocity and yaw rate from time step $k-1$ to time step k. This idea is illustrated in Fig. 2. The movement of a vehicle with constant forward velocity U from time $k-1$ to time k is given simply by $\Delta X, \Delta Y, \Delta\psi$ where X and Y are aligned with x and y at time step $k-1$. Those small motions are approximately given by

$$\Delta x = UT;\ \Delta y = V_{k-1}T;\ \Delta\psi = r_{k-1}T \quad (2)$$

when the time step T is small. When a simple coordinate transformation inclusive of the rotation $\Delta\psi$ is considered, the nonlinear equations expressing the globally stationary point P from the transformed local vehicle-fixed coordinate system at time k are given by (3). The notation $x_{i,j}$ indicates the relative forward spatial location x of the road point assumed to pass under the vehicle at i time steps in the future given time index j.

$$\begin{aligned} x_{p,k} &= (x_{p+1,k-1} - \Delta x)\cos\Delta\psi + (y_{p+1,k-1} - \Delta y)\sin\Delta\psi \\ y_{p,k} &= -(x_{p+1,k-1} - \Delta x)\sin\Delta\psi + (y_{p+1,k-1} - \Delta y)\cos\Delta\psi. \end{aligned} \quad (3)$$

Considering that most vehicles are only capable of $r < 60^{\circ/s}$ in yaw and that common time steps T for a filter of this nature are on the order of 0.02 s, a vehicle could only reasonably achieve a $\Delta\psi$ of approximately 2° from time step to time step, which falls well under the definition of small angles. Using the small angle assumption for the small movement of each point in the state vector between successive samples and recognizing that, in this framework, $x_{p+1,k-1} = (p+1)UT$, these equations lose their trigonometric terms, the following is obtained:

$$\begin{aligned} x_{p,k} &= ((p+1)UT - UT) + (y_{p+1,k-1} - V_{k-1}T)r_{k-1}T \\ y_{p,k} &= -((p+1)UT - UT)\, r_{k-1}T + (y_{p+1,k-1} - V_{k-1}T). \end{aligned} \quad (4)$$

Then, neglecting the small multiplicative nonlinear terms $-V_{k-1}r_{k-1}T$ and $y_{p+1,k-1}r_{k-1}T$, the x-position of the road at p time steps ahead, given current time k, becomes $x_{p,k} = pUT$. This is equivalent to the assumption that the road points "move toward the vehicle" with a velocity approximately equal to U from the vehicle's perspective. The relationship between the road y-offset at time $k-1$ and the y-offset of that *same* point at time k is given by

$$y_{p,k} = y_{p+1,k-1} - V_{k-1}T - r_{k-1}pUT^2. \quad (5)$$

Assembling the road edge dynamics under this new motion model, an open-loop discrete-time motion model is obtained. This is shown in (7). There, A_d and B_d are the corresponding matrix elements from the discrete A and B matrices derived using a Tustin discretization of (1). This augmented system represents the backward propagation of road geometry states toward the vehicle using a unit delay operator. It maintains all previewed road states in the state vector and is called a "shift register" by Sharp and Valtetsiotis in [22]. It will also be referred to as a shift register for the duration of this paper. The state equations are excited by three inputs: the vehicle steer angle δ, the road superelevation e, and the lateral position of the farthest road point on the N-time-step preview horizon, $m_{N-1,k}$, obtained from a preexisting map of road geometry.

C. Kalman-Filter Design

Road position measurements come from a camera which—because it is fixed to the windshield of the vehicle adjacent to the rear-view mirror—is always assumed to measure road geometry in the vehicle-fixed reference frame. Since each road point's motion is coupled to the vehicle motion, the measurement equation giving $\vec{z}_k$ in (7) for this estimator is quite simple. The vehicle's lateral velocity V and yaw rate r are both observable if the yaw rate and/or road points are available for measurement. The observability of the road geometry states is determined by the farthest road point available for measurement by the camera. Note, however, that a filter without measurements all the way out to the preview horizon will still "see" road geometry because the mapped road input is propagated toward the vehicle from the road, steering, and superelevation inputs $m_{N-1,k-1}$, δ, and e along with estimates of V and r.

The explicit relationship between the signals and operators in the preview-filter system is given in Fig. 3, which shows how local estimates of nonpreviewed vehicle states are fed back into the map registration procedure along with coarse longitudinal registration from GPS or an alternative odometric algorithm to obtain $m_{N-1,k-1}$ through a coordinate transformation. This will be explained in detail in the following section. Note that Fig. 3 shows a time-varying observer gain L_k. In practice, L_k is updated according to the standard current-

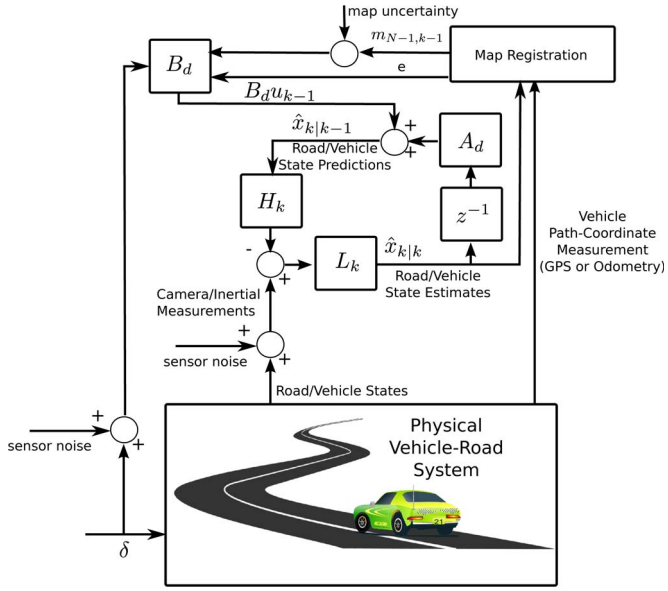

Fig. 3. Block diagram layout of preview filter.

measurement Kalman-filter equations as derived in [28] and shown briefly with time-varying system and measurement matrices in

$$\begin{aligned} \hat{x}_{k|k-1} &= A_{d,k-1}\hat{x}_{k-1|k-1} + B_{d,k-1}u_{k-1} \\ P_{k|k-1} &= A_{d,k-1}P_{k-1|k-1}A_{d,k-1}^T + Q_k \\ \tilde{y}_k &= z_k - H_k\hat{x}_{k|k-1} \\ L_k &= P_{k|k-1}H_k^T\left(H_kP_{k|k-1}H_k^T + R_k\right)^{-1} \\ \hat{x}_{k|k} &= \hat{x}_{k|k-1} + L_k\tilde{y}_k \\ P_{k|k} &= (\mathbb{I} - L_kH_k)P_{k|k-1} \end{aligned} \quad (6)$$

where the standard Kalman-filter terms are defined in [28] and A_d and B_d are defined in (7).

Because the filter assumes that the forward speed of the vehicle, U, is constant, if there are periods of abrupt acceleration, then the linear-time-varying filter structure presented here will likely not function properly. This can be corrected by changing the measurement equations and state transition equations to allow for varying spatial intervals in the preview horizon to maintain even temporal intervals based on a model for vehicle longitudinal acceleration. While this would be fairly straightforward to implement, it is not demonstrated here as the aim of this paper is to introduce the map-based estimator, and thus, the focus is to provide lateral vehicle and environment states during cruising.

D. Map Integration Through Road Input $m_{N-1,k-1}$

Because a map of road geometry is available, the map information can be used to generate a suitable vehicle-referenced $m_{N-1,k-1}$ value at time $k-1$ by aligning the road marker map with the vehicle coordinate frame through a basic coordinate transformation. This step provides an input to the road geometry motion model as shown analytically in Fig. 3 and allows the road line offset to propagate backward toward the vehicle as time marches forward. Lane position estimates are then updated by the camera measurements when available as (7), shown at the bottom of the next page.

Because road edge states are maintained in the filter structure in vehicle-fixed coordinates, the map registration in the global reference frame must be accomplished through a parallel process outside the Kalman filter of (6). This is illustrated in Fig. 4 and reflected in the signal diagram shown in Fig. 3. Vehicle yaw offset from the lane line tangent, defined in

$$\psi_{rel} \approx \frac{\hat{y}_{1,k-1} - \hat{y}_{0,k-1}}{UT} \quad (8)$$

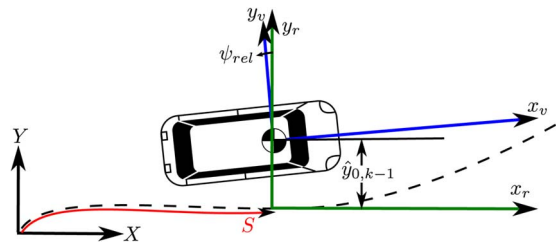

Fig. 4. Map registration procedure for local-coordinate preview estimator.

TABLE I
REPRESENTATIVE FILTER PARAMETERS

	Value	Units		Value	Units
σ^2_{gyro}	0.0066	$\frac{rad^2}{s^2}$	m	2579	kg
$\sigma^2_{S_{vehicle}}$	1.5	m^2	I_z	5411	kgm^2
$\sigma^2_{cam,x}$	$(1.5x^3 + 6.5x^2$		a	1.39	m
	$+57x) \times 10^{-6}$		b	1.964	m
	$+0.1$	m^2	C_r	-83700	$\frac{N}{rad}$
θcam	.035	rad	C_f	-75700	$\frac{N}{rad}$
h_{cam}	1.51	m			

and lateral position from the lane marker nearest the vehicle center of gravity (CG), given by y_0, are available in the augmented state vector. Then, the vehicle's global yaw angle is given by $\psi = \psi_r - \psi_{rel}$, with ψ_r representing the mapped road tangent angle as shown in Fig. 4. The estimator uses a road map where the station S_r or total distance traveled along the road is available in the map along with the Cartesian position (X_r, Y_r, Z_r) and orientation of the mapped lane marker $(\phi_r, \theta_r, \psi_r)$ at a number of discrete points. The use of the path coordinate S_r (generally referred to as "odometry" in Fig. 3) allows for a 1 : 1 lookup of the road marker pose, even for closed paths. At each time step, an independent measurement of S_r is used to find the nearest location of the vehicle in the map in path coordinates. Specifically, a K-nearest neighbors search registers a low-cost GPS position measurement to the map. Then, using the interpolation of the map points and simple coordinate transformation equations, the positions of the lane points within the preview horizon are computed in current "road frame" coordinates as shown in Fig. 4. Finally, the transformation from the road-aligned coordinate frame to the vehicle-fixed coordinate frame is achieved using the lateral offset of the vehicle from the lane line, given by $\hat{y}_{0,k-1}$ and a simple estimate of the vehicle's yaw offset from the road tangent, given by (8), thus obtaining the value of $m_{N-1,k-1}$.

Using a low-cost GPS sensor to obtain a longitudinal position estimate for the vehicle does introduce errors in $m_{N-1,k-1}$ for sharp curves or for abrupt changes in lane geometry, as expected. However, these errors are quickly corrected by camera measurements when available. Furthermore, the low-cost GPS sensor used in the experimental results (shown shortly) performed adequately for longitudinal map registration, and the occasional low-frequency bias errors of 1 to 3 meters found through extensive testing appeared to have little influence on the accuracy of the filter with respect to nonpreviewed states. This is largely a result of two effects: 1) The filter's weighting of the road edge information far in front of the vehicle for use in current lateral state estimation is relatively small, and 2) roads are generally painted so that contiguous lane markers do not have large changes in lateral position with respect to short longitudinal distance increments.

E. Preview Measurements and Noise Model

The following section explains how camera measurements are brought into the filter for the measurement update step of the Kalman filter as described by (6). To give appropriate weights to the lane measurements in the Kalman-filter structure at each previewed time, a basic noise model reflecting the physical uncertainty of a monocular camera extracting lane lines ahead of the vehicle is now considered. Any number of lane extraction techniques could be used for a filter of this type, and some of these may increase lane extraction accuracy, like those in [14] with built-in stabilization. Even stereo vision-based lane detection techniques would work, as in [2] or others, and some may be more robust to nonplanar road geometry in the preview horizon. The estimation strategy developed in this paper is flexible to implementations where multiple lane features are to be tracked (other lines, pavement irregularities, etc.), as long as the mapped features are stored with relative offsets from the lane center. However, for demonstration purposes, a simple canny edge detector was used to extract lane features.

The inverse perspective equations used to project identified pixel coordinates of lane features into the vehicle-fixed frame assume that the road in front of the vehicle is flat. This is inherently limiting but representative of many common lane measurement methods [13]. To model the expected noise in the lane position measured at each preview distance, the road surface area captured by each pixel was computed as a function of the preview distance for a VGA monochrome camera with a downward tilt angle θ_{cam} of 2° and a focal length f of 1068 pixels mounted at 1.57 m above an ideal flat road surface. A third-order polynomial fit of the total pixel area on the road surface versus the preview distance was used as a basis for the diagonal measurement noise matrix R_k in the Kalman filter of (6) and is shown in Table I. In addition, this model for lane feature measurement also neglects

$$[\vec{x}_k] = \underbrace{\begin{bmatrix} [A_d] & [0_{2\times N}] \\ \begin{bmatrix} -T & 0 \\ -T & -UT^2 \\ \vdots & \vdots \\ -T & -(N-2)UT^2 \\ 0 & 0 \end{bmatrix} & \begin{bmatrix} 0_{N-1\times 1} & \mathbb{I}_{N-1\times N-1} \\ 0 & 0_{1\times N-1} \end{bmatrix} \end{bmatrix}}_{A_a} \underbrace{\begin{bmatrix} V_{k-1} \\ r_{k-1} \\ y_{0,k-1} \\ y_{1,k-1} \\ \vdots \\ y_{N-2,k-1} \\ y_{N-1,k-1} \end{bmatrix}}_{\vec{x}_{k-1}} + \underbrace{\begin{bmatrix} B_d & 0 \\ 0 & 0 \\ \vdots & \vdots \\ 0 & 1 \end{bmatrix}}_{B_a} \underbrace{\begin{bmatrix} \delta \\ e \\ m_{N-1,k-1} \end{bmatrix}}_{u_{k-1}}$$

$$\vec{z}_k = \underbrace{\begin{bmatrix} 0 & 1 & 0_{1\times N} \\ 0 & 0 & \mathbb{I}_{N\times N} \end{bmatrix}}_{H} [\vec{x_k}]. \tag{7}$$

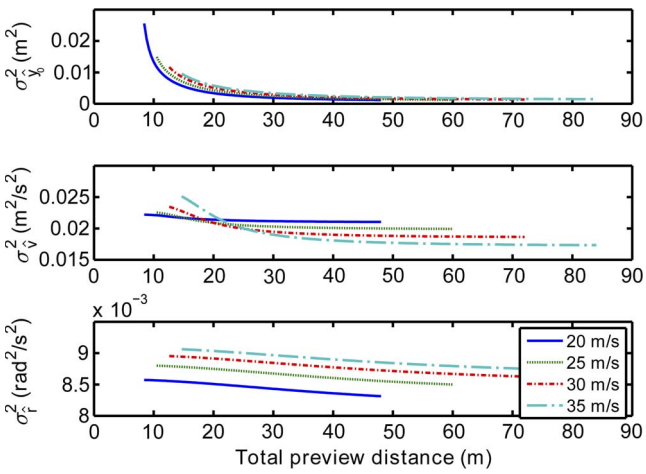

Fig. 5. Variance of vehicle states versus preview distance.

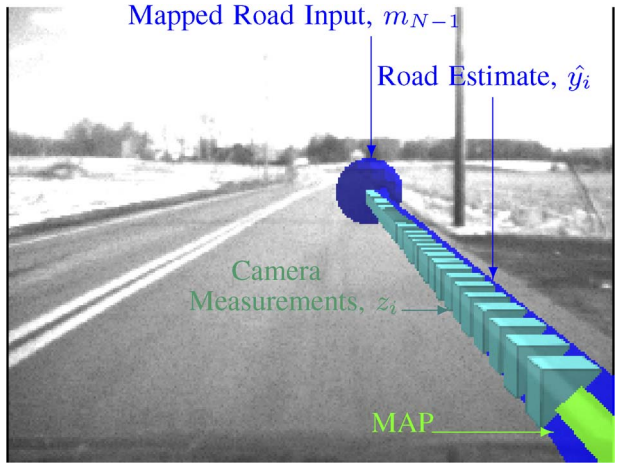

Fig. 6. Filter results overlaid with camera image, 55 mph.

the suspension motion of the vehicle leading to small changes in camera pose over bumps and when steering, throttle, or brake inputs cause roll, pitch, or heave motion of the suspension. To help mitigate this method's limitations, contributions of suspension motion and road profile irregularities to camera measurement errors were lumped into an inflated constant Gaussian noise term in the Kalman-filter framework. This value is also shown in Table I as the constant term at the end of the equation for $\sigma^2_{cam,x}$. Because a yaw rate measurement was also used, Table I also provides a representative Gaussian white noise parameter for an L3G4200D micro-electromechanical system gyroscope.

Finally, because map registration must be achieved through a measurement of distance traveled in the S direction, there will be noise in the vehicle's estimated distance along the road, $S_{vehicle}$. This causes process noise affecting $m_{N-1,k-1}$ in the filter design. The magnitude of the variance in $S_{vehicle}$, 1.5 m^2, was chosen using values reported in [29].

III. Theoretical Estimator Performance

The estimator performance will change with increasing preview distance and vehicle speed. To examine these effects, a series of steady-state Kalman filters was designed using increasing numbers of preview measurements for various fixed speeds. While the filter was not implemented as a steady-state estimator in practice, a steady-state analysis allows for *a priori* predictions of estimator performance, which could aid a perception or control system designer in selecting the correct sensors or setting a threshold for minimum visibility to enable autonomous lane keeping. The resulting filters were used to examine the steady-state covariance in each state estimate. These covariance values are illustrative in that they represent the achievable accuracy for a preview filter of a finite order for a given look-ahead condition. These results thus estimate an analytical relationship between look-ahead distance and achievable lateral state estimation accuracy.

The camera measurements of a road lane line in front of the vehicle were assumed to be no closer than 2 m from the vehicle's CG to account for the vehicle's body obscuring the ground directly under the vehicle. The camera noise parameters derived earlier for a typical monocular camera arrangement were held constant for each filter. The filters were designed for a vehicle with parameters given in Table I at constant forward speeds of $U = 20$ m/s to 35 m/s, which represent a range of speeds expected during highway driving. The resulting theoretical steady-state covariances on each state as a function of preview distance for each test speed are given in Fig. 5.

Fig. 5 shows that very good accuracy can be expected when using previewed lane line position and yaw rate alone for vehicle state estimation, even on difficult to estimate states like lateral velocity. The plot also indicates that an increasing number of temporally previewed features does, in general, benefit the task of vehicle state estimation. However, the figure also indicates that measurements of lane position at distances greater than 20 m become less useful for improving vehicle lateral position accuracy across highway driving speeds, at least for this specific camera and gyroscope arrangement.

The effect of vehicle speed on predicted estimator accuracy is also apparent in Fig. 5. Low speeds tend to give better estimator performance on the nonpreviewed road offset y_0. This is primarily due to the fact that, for a finite filter dimension, which represents a particular look-ahead *time*, higher speeds mean looking father out in front of the vehicle in *distance*. These distant camera measurements contain more noise, which is reflected in the Kalman filter. This illustrates a tradeoff between accuracy and simplicity—keeping the number of states in the estimator the same across speeds means looking farther ahead at higher speeds but at a more coarse distance interval. The trend of increasing speed decreasing accuracy is echoed in yaw rate estimation as well, as seen in Fig. 5. Interestingly, lateral velocity estimation accuracy actually increases with increasing speed. This is likely due to the fact that lateral velocity magnitudes are small at low speeds and grow with higher speeds; for most vehicles, the signal-to-noise ratio of lateral velocity increases with increasing speed.

While this *a priori* analysis is useful for seeing trends in how vehicle speed and look-ahead distance may affect estimator accuracy, the reader should tread carefully when interpreting the performance predictions in Fig. 5 literally. In practical implementations of the filter, not all previewed states will be available for measurement at all time steps, and unmodeled camera and vehicle dynamics could contribute significantly to error. Suspension-induced motion of the camera could distort lane measurements, tire nonlinearities could corrupt the model-based Kalman-filter estimates, and very large longitudinal map registration error could affect the road input $m_{N-1,k-1}$ significantly. Fortunately, the filter weights lane measurements close to the vehicle far more than measurements that are far in the future, and thus, these effects are small, as shown in the following section.

IV. Validation and Error Analysis

With the derivation of the filter equations in vehicle-fixed coordinates as described earlier, the estimator is readily applied to collected

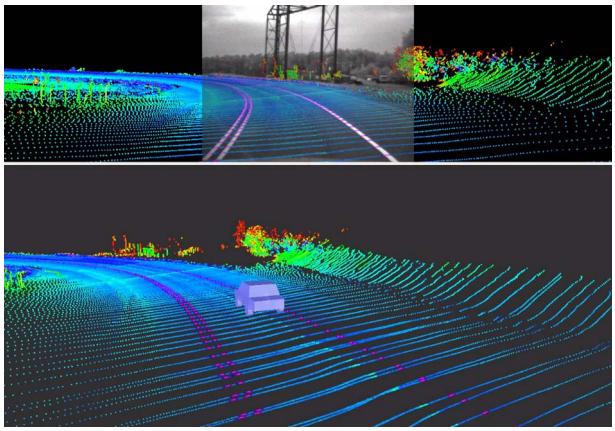

Fig. 7. Mapping of the Penn State test track.

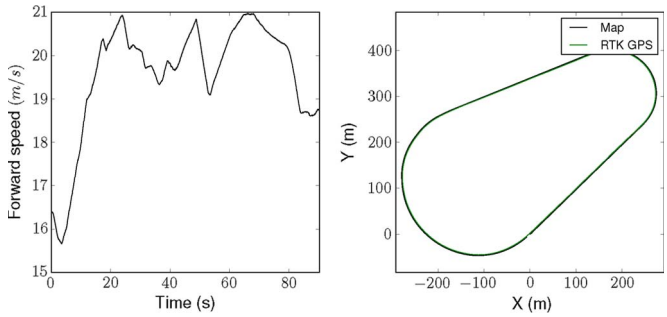

Fig. 8. Test trajectory and speed profile.

video, odometric, and inertial data to estimate vehicle states during live driving. Fig. 6 shows a sample of the match between an actual forward-looking camera image and the mapped lane feature (right lane line) obtained using a preview filter during a straight-road traversal. The visual agreement between the camera image and mapped lane geometry indicates a good estimate of local (and thus global) vehicle yaw angle and lateral position. The filter implemented used $N = 50$ and $T = .02$ s to put the preview horizon at 1 s, offering the majority of the accuracy benefits of preview for the camera used, according to Fig. 5.

A. Map Generation

Maps were generated using the RTK GPS/INS system and a downward-facing Sick LMS500 LIDAR sensor. Lane edges were extracted from the LIDAR data using a threshold on infrared reflectivity. At Pennsylvania State University's Larson Transportation Institute test track, multiple laps were performed to ensure repeatability in the mapping process and to confirm the fidelity of the Novatel Span DL4 GPS/INS system. A sample overlay of mapped LIDAR points onto the forward-looking camera image during the high-fidelity mapping is shown in Fig. 7.

Instead of saving all mapped intensities and positions in a grid, as is the standard for many of the map-based localization and tracking approaches, only a very compact version of the map is saved, representing just the right lane marker edge's position, extracted using a thresholding algorithm from LIDAR intensity data. Vehicle parameters for "Big Red," the General Motors Corporation (GMC) pickup used in this paper, are given in Table I.

B. Test Description

To test the potential accuracy of the preview filter framework in an environment with 3-D road geometry and realistic turns, a test

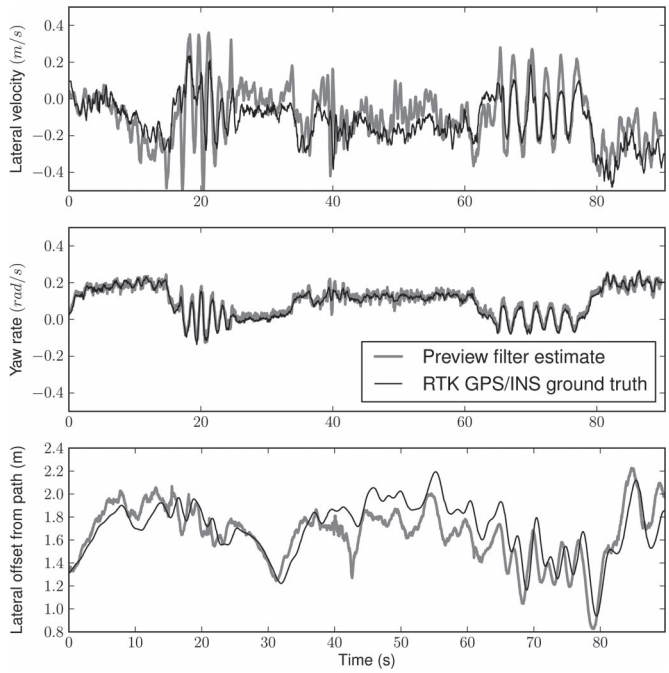

Fig. 9. State estimates versus ground truth for test track data.

was performed at The Larson Transportation Institute test track in Bellefonte, PA. While a test track cannot represent all public road situations, this test track is a challenging venue for lane-tracking algorithms since its one mile loop includes increasing, decreasing, and constant radii, along with a combination of asphalt and concrete pavement and significantly superelevated turns (6%–8%). The vehicle speed during this test was roughly 20 m/s throughout the traversal. The test included sinusoidal steering on several of the straight sections of the road to excite the vehicle dynamics for the purposes of testing the preview filter. Fig. 8 shows the ground-truth position trace and map for the counterclockwise validation run around the test track, along with the forward speed of the vehicle during the test. The estimator's performance using production-grade GPS and yaw-rate sensors was compared with a defense-grade factory-integrated INS system with differential corrections for the validation of the filter. As Fig. 8 indicates, the speed during the test was not entirely constant, but the driver attempted to maintain a fairly constant speed throughout the entire loop. Because additional lane tracking algorithms were not available for real-time implementation during the test, these results cannot address how the preview estimator performs relative to other systems. However, the test does provide a look at the accuracy of the system relative to an industry-standard ground-truth system.

C. Results

Fig. 9 shows the lateral velocity, yaw rate, and lateral position match between the ground-truth INS system and the preview filter for one mile-long lap of the test track. The course consists of two straightaways and two turns, each to the left and heavily banked. In the straightaways, the vehicle was intentionally steered with a sine wave-type pattern to test whether the estimator would work in both steady-state and transient maneuvers. While the overall agreement is good, scale-factor errors are present in the vehicle model, causing the overprediction of $\hat{V}$ as seen in Fig. 9. This, in turn, causes input-correlated noise in Fig. 10. These scale-factor errors in transient maneuvers are common in vehicle dynamic model predictions and are usually caused by unmodeled tire or suspension dynamics [30].

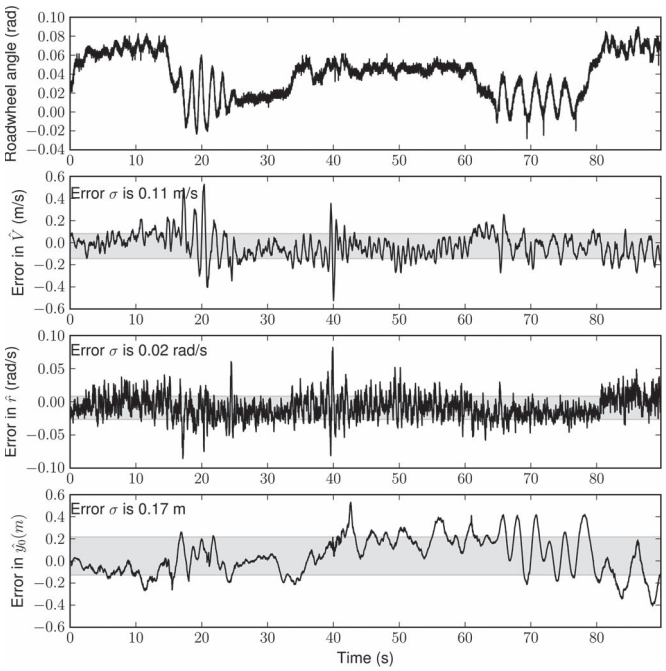

Fig. 10. Error in planar vehicle states for test track data.

Between approximately 0 and 15 s, the vehicle is in a steady-state turn with a yaw rate of 0.2 rad/s. According to Table I and the vehicle model, this should result in a steady-state lateral velocity of nearly 0.7 m/s, whereas a value near 0 m/s is measured. This discrepancy is because of the superelevation of the test track. Without inclusion of this mapped effect, there would be much worse agreement between the ground-truth value of V obtained from the INS system and the filter estimate $\hat{V}$.

The lateral offset, too, matches very well with the INS ground-truth data for the run, although the estimator performance bounds suggested in Section III are not quite achieved. This is to be expected, given the vehicle model errors and planar road approximations mentioned previously. The relative accuracy of the filter given its simplicity is notable.

To examine the performance of the filter, the error characteristics of the vehicle state estimates are shown in Fig. 10. The errors are agreeably small in maximum and in standard deviation, but there appear to be systematic components in $\hat{V}$ and $\hat{y}_0$, which may stem from measurement model error (e.g., approaching nonflat portions of the track, roll motion of the vehicle, etc.) or errors in timing. In regard to $\hat{y}_0$, recall that the forward-looking camera cannot see the road directly underneath the vehicle; close lane position estimates are obtained by propagation without corrections for the 2 m closest to the vehicle. Thus, small errors in U, longitudinal acceleration or deceleration, synchronization errors, and other unmodeled error sources in the camera measurement step may contribute to lateral position error.

To address the way that the filter functions in the measurement update step, the innovations were examined for the test run. Kalman filters are assumed to have zero-mean innovations with white noise characteristics when operating on a true linear system perturbed by unbiased Gaussian noise. To examine the mean and standard deviation of the innovations at each preview point for the whole run, consider Fig. 11, which shows that innovations out to preview point 40 (0.8 s or 16 m in front of the vehicle) are nearly zero mean but, beyond this point, innovations are biased. This is an artifact of a mean bias in the GPS-based longitudinal map registration. Because the weight on measurements beyond 20 m is quite small due to the camera noise

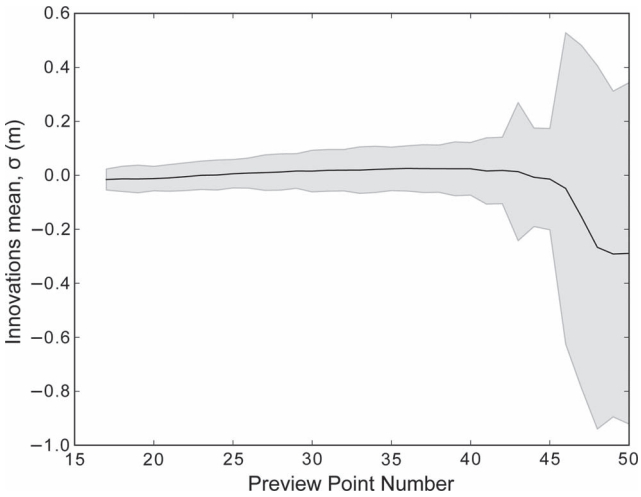

Fig. 11. Measurement innovations for all preview points.

model, this bias does not introduce significant biases into the filtered estimate of roadway geometry or vehicle states.

The robustness of this estimator in the presence of missing lane measurements is notable. Due to the intentionally crude lane detector used in this study, between 10 and 45 of the 50 preview samples were missing for each update step in the test track runs. These missing data caused little degradation in filter performance. Furthermore, the number of missing samples appeared to correlate strongly with particular positions in the track, suggesting that such errors can be mapped as well for later inclusion in the filter structure. Complete tests of the filter's inherent robustness to occlusion and position-specific error correlation are areas of ongoing study.

V. Conclusion

This paper presented a novel flexible filter framework for improving vehicle state estimates and estimates of windowed road geometry using a camera and a map. Application of this filter structure to real driving data shows that the effect of superelevation on estimator performance is significant. Errors in the experimental performance appear to be most strongly related to unmodeled vehicle dynamics. Experimental and theoretical analysis both show that the benefits of state estimation using previewed lane geometry improve with increasing lane preview, but this improvement diminished due to increased lane tracking errors at distances beyond 20 m ahead of the vehicle.

References

[1] E. Dickmanns and H. Wünsche, *Dynamic Vision for Perception and Control of Motion*. New York, NY, USA: Springer-Verlag, 2007.

[2] M. Bertozzi and A. Broggi, "Gold: A parallel real-time stereo vision system for generic obstacle and lane detection," *IEEE Trans. Image Process.*, vol. 7, no. 1, pp. 62–81, Jan. 1998.

[3] J. McCall and M. Trivedi, "Video-based lane estimation and tracking for driver assistance: Survey, system, evaluation," *IEEE Trans. Intell. Transp. Syst.*, vol. 7, no. 1, pp. 20–37, Mar. 2006.

[4] V. Kastrinaki, M. Zervakis, and K. Kalaitzakis, "A survey of video processing techniques for traffic applications," *Image Vis. Comput.*, vol. 21, no. 4, pp. 359–381, Apr. 2003.

[5] M. Bertozzi, A. Broggi, and A. Fascioli, "Vision-based intelligent vehicles: State of the art and perspectives," *Robot. Auton. Syst.*, vol. 32, no. 1, pp. 1–16, Jul. 2000.

[6] I. Parra Alonso *et al.*, "Accurate global localization using visual odometry and digital maps on urban environments," *IEEE Trans. Intell. Transp. Syst.*, vol. 13, no. 4, pp. 1535–1545, Dec. 2012.

[7] O. Pink, "Visual map matching and localization using a global feature map," in *Proc. IEEE CVPR Workshops*, 2008, pp. 1–7.

[8] C. Cappelle, M. El Badaoui El Najjar, D. Pomorski, and F. Charpillet, "Localisation in urban environment using GPS and INS aided by monocular vision system and 3D geographical model," in *Proc. IEEE IVS*, 2007, pp. 811–816.

[9] V. Gupta and S. Brennan, "Terrain-based vehicle orientation estimation combining vision and inertial measurements," *J. Field Robot.*, vol. 25, no. 3, pp. 181–202, Mar. 2008.

[10] M. Noda *et al.*, "Vehicle ego-localization by matching in-vehicle camera images to an aerial image," in *Proc. ACCV Workshops*, 2011, pp. 163–173, Springer.

[11] A. Vu, A. Ramanandan, A. Chen, J. Farrell, and M. Barth, "Real-time computer vision/DGPS-aided inertial navigation system for lane-level vehicle navigation," *IEEE Trans. Intell. Transp. Syst.*, vol. 13, no. 2, pp. 899–913, Jun. 2012.

[12] N. Mattern and G. Wanielik, "Camera-based vehicle localization at intersections using detailed digital maps," in *Proc. IEEE PLNS*, 2010, pp. 1100–1107.

[13] H. Cheng, "Road Detection and Tracking," in *In Autonomous Intelligent Vehicles*. London, U.K.: Springer-Verlag, 2011, pp. 33–59.

[14] M. Nieto, L. Salgado, F. Jaureguizar, and J. Cabrera, "Stabilization of inverse perspective mapping images based on robust vanishing point estimation," in *Proc. IEEE IVS*, 2007, pp. 315–320.

[15] D. Schreiber, B. Alefs, and M. Clabian, "Single camera lane detection and tracking," in *Proc. IEEE ITS*, 2005, pp. 302–307.

[16] Y. Lee *et al.*, "Adaptive localization for mobile robots in urban environments using low-cost sensors and enhanced topological map," in *Proc. IEEE ICAR*, 2011, pp. 569–575.

[17] M. J. Milford and G. F. Wyeth, "Single camera vision-only SLAM on a suburban road network," in *Proc. IEEE Int. Conf. Robot. Autom.*, 2008, pp. 3684–3689.

[18] L. Clemente, A. Davison, I. Reid, J. Neira, and J. Tardós, "Mapping large loops with a single hand-held camera," in *Proc. Robot.: Sci. Syst. Conf.*, 2007, pp. 1–8.

[19] J. Levinson, M. Montemerlo, and S. Thrun, "Map-based precision vehicle localization in urban environments," in *Proc. Robot.: Sci. Syst. Conf.*, 2007, pp. 1–8.

[20] M. Montemerlo, S. Thrun, D. Koller, and B. Wegbreit, "FastSLAM: A factored solution to the simultaneous localization and mapping problem," in *Proc. AAAI/IAAI*, 2002, pp. 593–598.

[21] A. Dean, R. Martini, and S. Brennan, "Terrain-based road vehicle localisation using particle filters," *Veh. Syst. Dyn.*, vol. 49, no. 8, pp. 1209–1223, 2011.

[22] R. Sharp and V. Valtetsiotis, "Optimal preview car steering control," in *Proc. ICTAM Sel. Papers 20th Int. Congr.*, P. Lugner and J. K. Hedrick, Eds., 2001, vol. 35, pp. 101–117.

[23] A. Pick and D. Cole, "Neuromuscular dynamics and the vehicle steering task," *Veh. Syst. Dyn.*, vol. 41, pp. 182–191, 2004.

[24] D. Cole, A. Pick, and A. Odhams, "Predictive and linear quadratic methods for potential application to modelling driver steering control," *Veh. Syst. Dyn.*, vol. 44, no. 3, pp. 259–284, 2006.

[25] A. Brown and S. Brennan, "Global and local frameworks for vehicle state estimation using temporally previewed mapped lane features," in *Proc. IEEE IVS Workshops*, 2013, pp. 127–133.

[26] H. Pacejka, *Tyre and Vehicle Dynamics*. Oxford, U.K.: Butterworth-Heinemann, 2005.

[27] C. Voser, R. Y. Hindiyeh, and J. C. Gerdes, "Analysis and control of high sideslip manoeuvres," *Veh. Syst. Dyn.*, vol. 48, no. S1, pp. 317–336, 2010.

[28] D. Simon, *Optimal State Estimation: Kalman, H Infinity, Nonlinear Approaches*. Hoboken, NJ, USA: Wiley, 2006.

[29] K. Jerath and S. Brennan, "GPS-free terrain-based vehicle tracking performance as a function of inertial sensor characteristics," in *Proc. ASME DSCC*, Arlington, VA, USA, 2011, pp. 367–374.

[30] S. Lapapong, A. A. Brown, and S. N. Brennan, "Frequency characteristics and explanation of notches seen in frequency responses of vehicles," in *Proc. TSME Int. Conf. Mech. Eng.*, Krabi, Thailand, 2011, pp. 1–8.